Article

Affects of Mechanical Milling and Metal Oxide Additives on Sorption Kinetics of 1:1 LiNH$_2$/MgH$_2$ Mixture

Donald L. Anton *, Christine J. Price and Joshua Gray

Savannah River National Laboratory/Aiken, SC 29803, USA; E-Mails: christine.erdy@srs.gov (C.J.P.); joshua.gray@srnl.doe.gov (J.G.)

* Author to whom correspondence should be addressed; E-Mail: donald.anton@srnl.doe.gov; Tel.: +1-803-507-8551; Fax: +1-803-652-8137.

Abstract: The destabilized complex hydride system composed of LiNH$_2$:MgH$_2$ (1:1 molar ratio) is one of the leading candidates of hydrogen storage with a reversible hydrogen storage capacity of 8.1 wt%. A low sorption enthalpy of ~32 kJ/mole H$_2$ was first predicted by Alapati *et al.* utilizing first principle density function theory (DFT) calculations and has been subsequently confirmed empirically by Lu *et al.* through differential thermal analysis (DTA). This enthalpy suggests that favorable sorption kinetics should be obtainable at temperatures in the range of 160 °C to 200 °C. Preliminary experiments reported in the literature indicate that sorption kinetics are substantially lower than expected in this temperature range despite favorable thermodynamics. Systematic isothermal and isobaric sorption experiments were performed using a Sievert's apparatus to form a baseline data set by which to compare kinetic results over the pressure and temperature range anticipated for use of this material as a hydrogen storage media. Various material preparation methods and compositional modifications were performed in attempts to increase the kinetics while lowering the sorption temperatures. This paper outlines the results of these systematic tests and describes a number of beneficial additions which influence kinetics as well as NH$_3$ formation.

Keywords: hydrogen storage; lithium amide; magnesium hydride; isothermal kinetics; oxide

1. Introduction

Development of high-performance on-board hydrogen storage systems are recognized as critical to implementation of hydrogen fuel cells as clean, efficient automotive power plants [1]. Among the various condensed phase storage system types—adsorbent materials, chemical hydrides and metal hydrides—the use of complex metal hydrides are being studied due to their combined favorable gravimetric and volumetric storage capacities [2], on-board reversibility, and indefinite ambient temperature storage duration.

In 2002, Chen *et al.* identified a hydrogen storage system based on the rehydrogenation of lithium nitride (Li_3N) in the following reactions [3]:

$$Li_3N + 2H_2 \Leftrightarrow Li_2NH + LiH + H_2 \Leftrightarrow LiNH_2 + 2LiH \tag{1}$$

Even though both steps are reversible and contain an overall hydrogen capacity of 11.5 wt%, a dehydriding enthalpy of ~66 kJ/mol H_2 [4] allows only the rightmost reaction to release hydrogen gas under practical conditions [1,5]. This is due to strong polar covalent bonds between hydrogen and nitrogen in NH^{2-} and to the strong ionic bonds that hold the H^- in the case of LiH [6].

With the substitution of LiH with MgH_2 and the subsequent destabilizing of the hydrogen bonds, the Li–Mg–N system has became one of the most promising systems with its relatively high hydrogen content and favorable thermodynamics [7,8]. Through the research of Luo [5,7,9] and Xiong [10], a 2:1 molar mixture of $LiNH_2$ and MgH_2, or the equivalent $Mg(NH_2)_2$ and 2LiH mixture due to the metathesis reaction between the two metal hydride – amide pairs which occurs at 220 °C under 100 bar of H_2 pressure [5,11], has been shown to have a theoretical hydrogen capacity of 5.5 wt% H_2. Both X-ray diffraction and IR spectroscopy [12] have shown that the overall reversible reaction can be written as:

$$2Li_2NH + MgH_2 \rightarrow Li_2Mg(NH)_2 + 2H_2 \Leftrightarrow Mg(NH_2)_2 + 2LiH \tag{2}$$
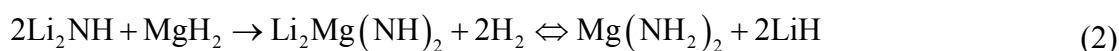
After 9 cycles, the 2:1 system has been shown to have a capacity of 4.59 wt% H_2 [7]. Through the use of deuterium absorption and in-situ neutron diffraction, the absorption reaction pathway was investigated by Weidner *et al.* [13] who observed that the immediate absorption reaction can be stated as:

$$2Li_2Mg(ND)_2 + 4D_2 \rightarrow LiD + LiND_2 + Li_2Mg(ND)_3 \rightarrow 4LiD + 2Mg(ND_2)_2 \tag{3}$$
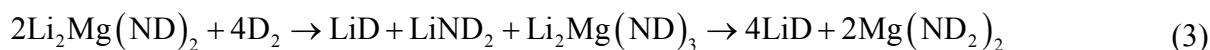
In a separate neutron diffraction study, Dolci *et al.* observed the formation of $LiNH_2$ and $Li_2Mg_2(NH)_3$ with an increase in the amount of LiH for desorbed material, $Li_2Mg(NH)_2$, at 200 °C and equilibrium pressures below 40 bar [14]. $Mg(NH_2)_2$ formation was not observed until the pressure was raised about 40 bar at 200 °C [14]. Araújo *et al.* predicted an enthalpy of 46.1 kJ/mol H_2 for the reversible reaction [6], which is slightly higher than the experimental values of 39 kJ/mol H_2 measured by Luo [7] and the 41.6 kJ/mol H_2 measured by Yang *et al.* [15].

In order to understand if the reaction was ammonia-mediated or a coordinated two-molecule or mutlimolecular reaction mechanism, Chen *et al.* performed both isothermal and non-isothermal kinetic measurements on the reaction between $Mg(NH_2)_2$ and LiH [16]. It was concluded that in the early stages of the reaction, the kinetic barrier may result from the interface reaction between the amide and

hydride; however, as the reaction progressed, the resistance of mass transport through the product layer increased and becomes the rate-determining step [16].

Different molar ratios of $Mg(NH_2)_2$ and LiH have also been explored for promising hydrogen storage systems. Leng *et al*. investigated the hydrogen desorption reaction between 8:3 LiH:$Mg(NH_2)_2$ mixture [8]. From TGA analysis, the first desorption of the milled 8:3 mixture resulted in hydrogen desorption starting at 140 °C at a heating rate of 5 °C/min with minimal ammonia release and 6.9 wt% hydrogen released by 400 °C. After heating the mixture to 400 °C, XRD revealed that the desorption reaction proceeds via:

$$3Mg(NH_2)_2 + 8LiH \rightarrow Mg_3N_2 + 4Li_2NH + 8H_2 \tag{4}$$

An XRD analysis has confirmed that the above reaction is reversible at 200 °C under 3 MPa of hydrogen [8,17]. However, during dehydrogenation at 250 °C, Aoki *et al*. observed that 5.1 mass% hydrogen had been desorbed [18]. The XRD spectra taken after dehydrogenation showed:

$$3Mg(NH_2)_2 + 8LiH \rightarrow 3Li_2Mg(NH)_2 + 2LiH + 6H_2 \tag{5}$$
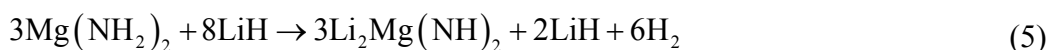
and that subsequent dehydrogenation of $3Li_2Mg(NH)_2$ was not observed at 250 °C, indicating that complete dehydrogenation to Mg_3N_2 and Li_2NH does not occur till higher temperature [18].

A two step dehydrogenation reaction was predicted for the 8:3 ratio: the first step being the conversion from $3Mg(NH_2)_2 + 8LiH$ to $3Li_2Mg(NH)_2 + 2LiH + 6H_2$ with an enthalpy of 46.1 kJ/mol H_2 and the second step being the final conversion to $4Li_2NH + Mg_3N_2 + 8H_2$ with an enthalpy of 84.1 kJ/mol H_2 [6]. Araújo *et al*. stated that if $Li_2Mg(NH)_2$ did not stabilize, the reaction enthalpy would be 55.6 kJ/mol H_2 [6].

When the ratio between $Mg(NH_2)_2$:LiH was increased to 1:4, the hydrogen capacity of the Li–Mg–N–H system increased to 9.1 wt% [19–21]. Reversible sorption is proposed to occur via the following reaction:

$$3Mg(NH_2)_2 + 12LiH \rightarrow Mg_3N_2 + 4Li_3N + 12H_2 \tag{6}$$

The dehydrogenation reaction has been observed to begin at approximately 227 °C at a heating rate of 10 K/min under 0.1 MPa of argon; however, only 8 mass% had been desorbed by 427 °C [21].

Aoki *et al*. investigated the dehydriding and structural properties of the 1:4 LiH:$Mg(NH_2)_2$ system under hydrogen pressure using the p-c isotherm measurement and XRD [18,19]. The total amount of desorbed hydrogen at 200, 225, and 250 °C were 4.5, 4.7, and 4.9 mass%, respectively with a calculated enthalpy of hydrogenation of −46 kJ/mol H_2 [19]. Based upon the XRD spectra after dehydrogenation at 250 °C under hydrogen pressure, the dehydrogenation process is proposed as:

$$3Mg(NH_2)_2 + 12LiH \rightarrow 3Li_2Mg(NH)_2 + 6LiN + 6H_2 \tag{7}$$
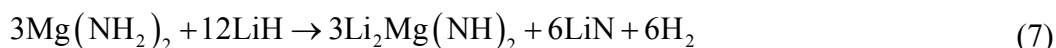
and there was no indication of further dehydrogenation of $3Li_2Mg(NH)_2$ [18].

In 2002, Alapati *et al*. predicted that the reaction between 1:1 MgH_2 and $LiNH_2$ was energetically favorable with an enthalpy of 31.9 kJ/mol H_2 through the use of first principle density function theory (DFT) [22]. The dehydrogenation reaction pathway is as follows:

$$LiNH_2 + MgH_2 \rightarrow LiMgN + 2H_2 \tag{8}$$

This mixture has a theoretical hydrogen weight capacity of 8.2 wt%.

Through a separate first-principle calculations of total energies and vibrations free energies, Akbarzadeh *et al.* suggested that the initial decomposition of 1:1 LiNH$_2$:MgH$_2$ will proceed as in a series of reaction steps [4]:

$$LiNH_2 + MgH_2 \rightarrow LiH + \frac{1}{2}Mg(NH_2)_2 + \frac{1}{2}MgH_2 \qquad (9)$$

$$\rightarrow LiH + \frac{1}{4}Mg(NH_2)_2 + \frac{1}{4}Mg_3N_2 + H_2 \qquad (10)$$

$$\rightarrow \frac{1}{2}LiH + \frac{1}{4}Mg_3N_2 + \frac{1}{4}Li_2Mg(NH_2)_2 + \frac{3}{2}H_2 \qquad (11)$$

$$\rightarrow LiMgN + 2H_2 \qquad (12)$$
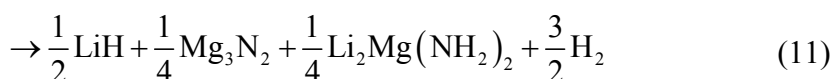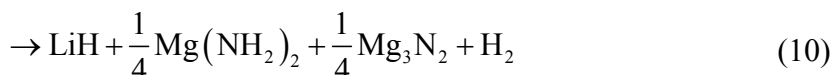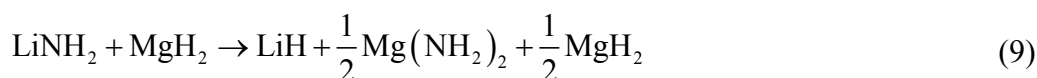
The formation of magnesium amide, which is the first step in the decomposition pathway, was predicted to be exothermic. In the next step Mg$_3$N$_2$ and H$_2$ would be formed from the MgH$_2$ and half of the Mg(NH$_2$)$_2$ in an endothermic reaction with an enthalpy of 15 kJ/mol H$_2$ [4]. A mixed Li–Mg imide would be produced in the next step with an enthalpy of 47 kJ/mol H$_2$ [4]. Finally, LiMgN is formed with an enthalpy of 80 kJ/mol H$_2$ at 227 °C [4].

Experimental, Lu *et al.* found that after jar rolling for 12 to 24 h, the 1:1 LiNH$_2$:MgH$_2$ mixture started to release hydrogen around 120 °C and released 8.1 wt% after being held at 220 °C for 20 min [23]. The material was able to successfully uptake 5 wt% when heated to 240 °C under 2000 psi [23]. With the addition of TiCl$_3$ as a modifier, the system was able to uptake 8/0 wt% from the rehydrogenation process at 2000 psi, 160 °C for 6 h [23,24]. The proposed rehydrogenation and subsequent dehydrogenation process of LiMgN produces LiH, Mg(NH$_2$)$_2$ and MgH$_2$, as [23]:

$$LiMgN + 2H_2 \leftrightarrow \frac{1}{2}Mg(NH_2)_2 + \frac{1}{2}MgH_2 + LiH \qquad (13)$$
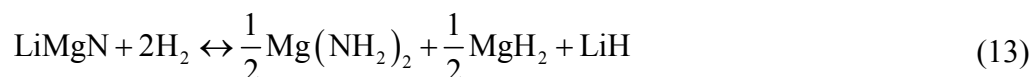
It has been further suggested by Luo *et al.* [21] that the rehydrogenation pathway is not directly back to the hydrogenated state, but via an intermediate hydride as given by:

$$LiMgN + H_2 \rightarrow Li_{2x}Mg_{1-x}(NH)_2 + MgH_2 + H_2 \rightarrow \frac{1}{2}Mg(NH_2)_2 + \frac{1}{2}MgH_2 + LiH \qquad (14)$$
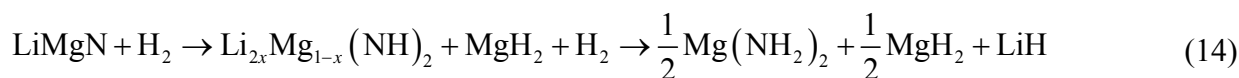
The mixture does not rehydrogenate back to LiNH$_2$ and MgH$_2$ but rather to LiH, MgH$_2$ and Mg(NH$_2$)$_2$ as shown in equation (4) [5].

Further investigations into the 1:1 system show that the kinetics and capacity are highly dependent on processing techniques and experimental conditions. In a study involving Fritsch milling, Liu *et al.* found that milling for 12 h resulted in LiH and Mg(NH$_2$)$_2$ formation with unreacted MgH$_2$ while milling for 36 h also formed MgNH [25,26]. This resulted in a reduction of the weight capacity to 6.1 wt%, a higher experimental enthalpy value of 45.9 kJ/mol H$_2$ and the formation of Li$_2$Mg(NH)$_2$, Mg$_3$N$_2$ and LiH after heating to 390 °C [25]. In another investigation into the 1:1 molar mixture, Osborn *et al.* milled the sample for 3 h under argon with a Szegvari attritor, which upon heating to 550 °C at 5 °C/min released 8.73 wt% [27]. Ammonia emission was found to begin around 260 °C with a concentration of 16.4 ppm mg^{-1}, which was attributed to the slow kinetics of converting NH$_3$ to

H_2 using MgH_2 [27]. Upon PCI measurements at 210 °C, only 3.4 wt% was released forming $Li_2Mg_2(NH)_3$ and LiH [27].

The observations cited above can be readily summarized by studying the quaternary phase diagram of the Li, Mg, N, H system given in Figure 1.

Figure 1. Pseudo quaternary phase diagram of the Li–Mg–N–H system showing relative phase compositions of known phases relevant to hydrogen sorption.
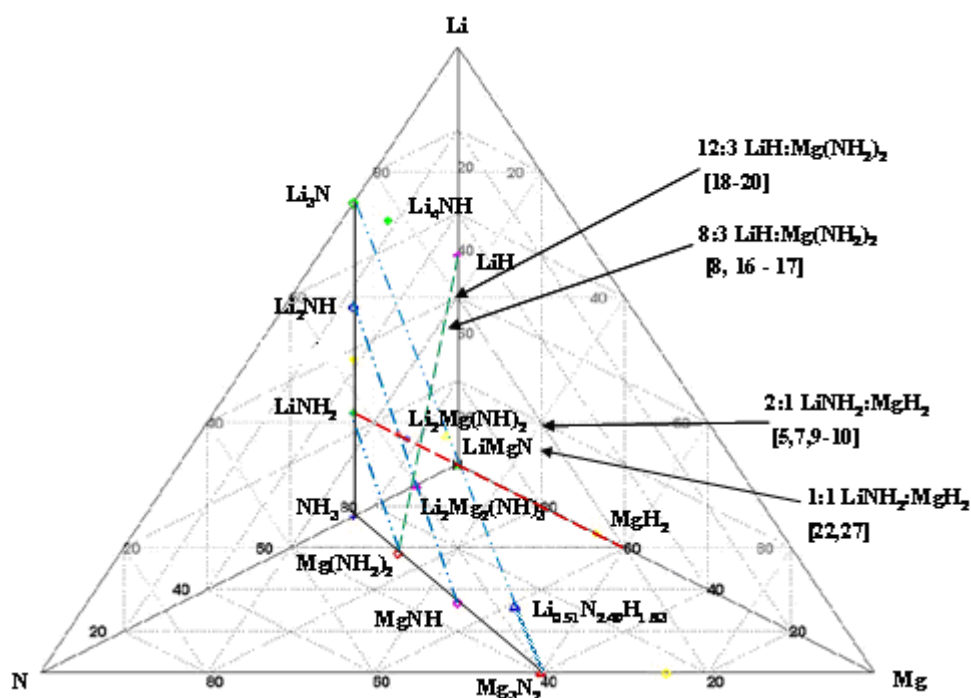
Here the ternary Li, N, Mg phase diagram is given in the plane of the page with hydrogen coming directly out of the page plane and lying directly above the ternary LiMgN phase. This ternary diagram is constructed by inserting all of the known phases by atom fraction for this system without regard to temperature or pressure, thus it is not an equilibrium phase diagram. The tie lines connecting Li_3N with NH_3 and Mg_3N_2 with NH_3 show the outer extreme of these ternary concentrations. Between these two tie lines one sees a plane of descending hydrogen concentration with its apex at NH_3 and descending through the amides $LiNH_2$–$Mg(NH_2)_2$, imides Li_2NH–MgNH and finally to the nitrides Li_3N–Mg_3N_2 .

Many of the recent publications on materials in this phase space have centered either on the $LiNH_2$:MgH_2 tie line at the 2:1 Li:Mg concentrations or along the LiH–$Mg(NH_2)_2$ tie line along the higher LiH concentrations. It is clearly shown that all compositions along this tie line will miss the LiMgN decomposition and likely result in one of the imides: Li_2NH, $Li_2Mg(NH)_2$ or $Li_2Mg_2(NH)_3$. At high $LiNH_2$ concentrations, dehydrogenation will result in composition to either $Li_2Mg_2(NH)_3$ or $Li_2Mg(NH)_2$. Through theoretically computed structural energetics, these compositions have been shown to be stable, $\Delta H_{T=500K}^{vib}$ = 128.5 and 200.7 kJ/mol H_2 [28], and not to give up further hydrogen at temperatures of potential utilization below 200 °C [5,7,9]. These structures have yet to be indentified experimentally. Similarly, with no Mg present, the terminal phase is the Li_2NH. However, with the additional of MgH_2, at the Li:Mg ratio of 1:1, these amine phases can be avoided resulting in the

terminal LiMgN and complete hydrogen release [23]. This decomposition has been shown to occur at temperatures as low at 120 °C and can be rehydrogenated under 138 bar [23]

In this paper, we investigate the base line isothermal and isobaric sorption kinetics of the 1:1 $LiNH_2$:MgH_2.composition. Qualitative gas stream chemistries were monitored to differentiate between hydrogen and ammonia discharge. The effects of various dopants on sorption rates, the temperature of initial hydrogen release and the amount of ammonia released were subsequently investigated. Implications for use of this material for hydrogen storage applications are summarized.

2. Results and Discussion

2.1. Unmodified System

2.1.1. Characterization of Unmodified As-Milled Material

The XRD pattern of the milled 1:1 molar mixture of $LiNH_2$ and MgH_2 revealed only the starting materials with no phase changes or reactions occurring during the milling process.

Figure 2. XRD pattern for the Fritsch milled (top) and Spex milled (bottom) samples.
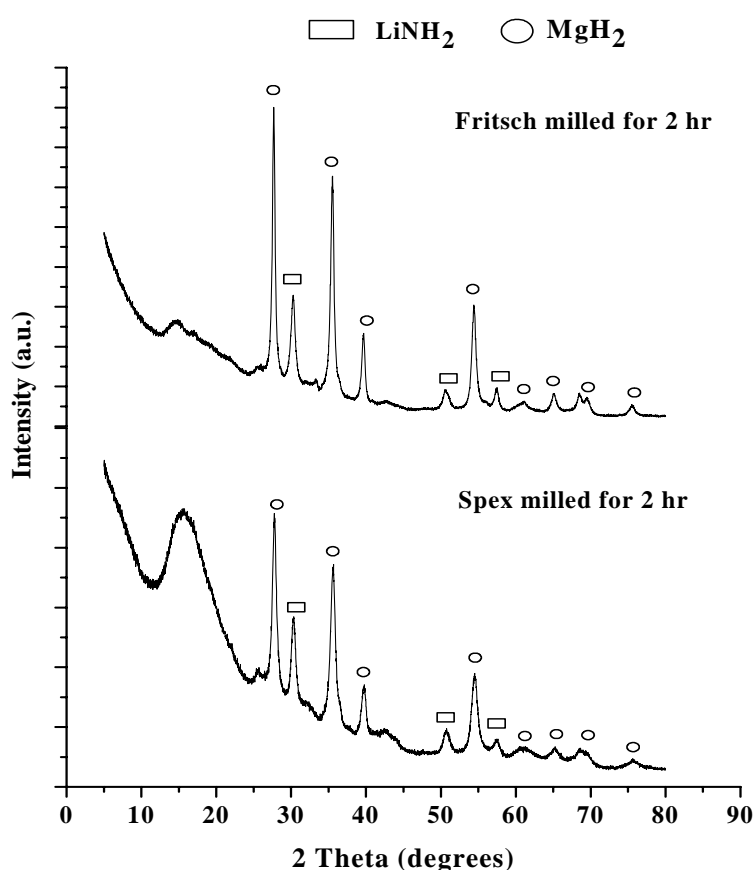
This is evident by the MgH_2 peaks, denoted by circles in Figure 2, and $LiNH_2$, denoted by rectangles. These results are similar to those observed by Liu *et al.* after milling for 2 h at 500 rpm on the Fritsch mill [25] and Lu *et al.* after milling for 30 min on the Spex mill [24]. The broad peak seen in the lower angle region is attributed to the kapton film used to prevent oxidation of the samples

during measurement. The pattern of the Spex milled sample did reveal peak broadening and lower intensity indicating a decrease in particle size and an increase in defects [29]. Using the Scherrer equation to determine particle size from XRD patterns, the average MgH_2 particle was reduced from 35.3 nm to 23.6 nm.

2.1.2. Decomposition Behavior of Unmodified As-Milled Material

As discussed in our previous publication [30] the unmodified Fritsch milled sample started to desorb hydrogen at approximately 135 °C during ramping from RT to 400 °C at with heating at a rate of 5 °C/min [30].

Figure 3. TGA curves for Fritsch (red) and Spex (blue) milled unmodified 1:1 $LiNH_2$:MgH_2 mixture. The apparent slight increase in mass observed at the start of heating is attributed to the expansion of the argon carrier gas.
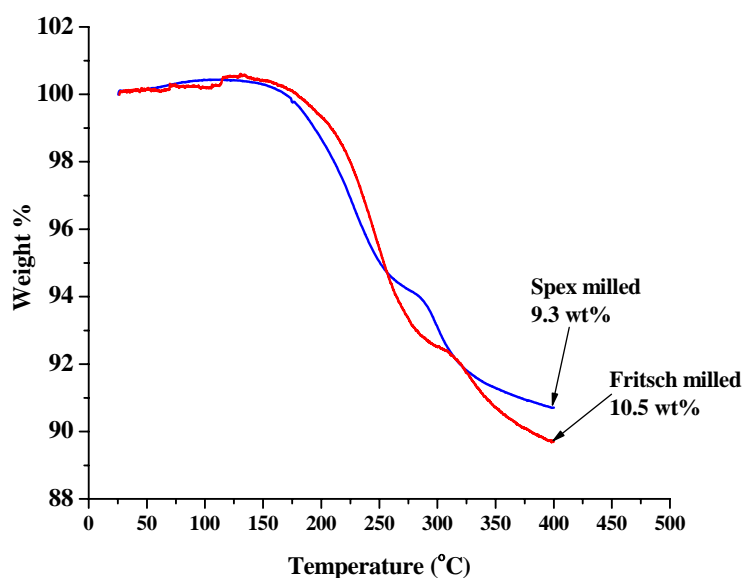
From the TGA results in Figure 3 and RGA data given in Figure 4A,B, hydrogen desorption for the Fritsch-milled unmodified material starts at approximately 135 °C with three hydrogen peaks at 205 °C, 260 °C, and 340 °C, indicating that the sample decomposed in three steps. It is possible to attribute these hydrogen releases to the decomposition reactions listed by Akbarzadeh *et al.* [4] as reviewed previously. An in-depth investigation of the dehydrogenation pathway is needed to confirm the proposed decomposition reactions. On the other hand, the Spex-milled material started to desorb hydrogen at approximately 120 °C resulting in two defined hydrogen peaks at 230 °C and 330 °C with a shoulder at 218 °C. This reduction in initial dehydrogenation temperature can be attributed to the smaller particle size resulting from Spex-milled samples which resulted in increased surface area and lower surface activation energy [29,31,32].

Figure 4. RGA results for (**A**) hydrogen and (**B**) ammonia for Fritsch (red) and Spex (blue) milled material.
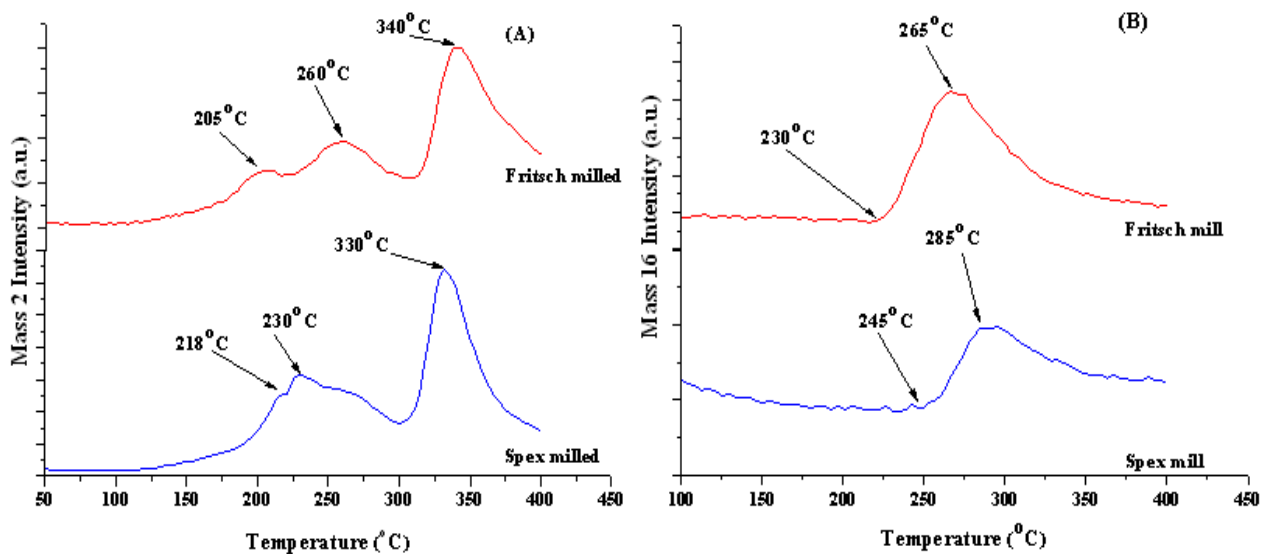
Ammonia release peaked at 265 °C for the Fritsch milled sample, as shown in Figure 4B. Similarly, the ammonia release from the Spex milled sample peaked at 285 °C. The source of ammonia can be attributed to the decomposition of unreacted $LiNH_2$, the slow reaction kinetics between MgH_2 and NH_3 from decomposing $LiNH_2$ [12,33,34] and/or the decomposition of $Mg(NH_2)_2$, which runs parallel to the H_2 desorption of the hydride-amide system [35]. Janot *et al.* showed that a mixture of 2:1 $LiNH_2$:MgH_2 lost significantly more weight than a 2:1 LiH:$Mg(NH_2)_2$ at 200 °C into primary vacuum due to ammonia release [12].

At the end of the decomposition, the total weight lost for the Fritsch milled sample was 10.5 wt%, and 9.3 wt% for the Spex milled sample. When comparing the predicted weight loss for each decomposition step to the observed weight loss, ammonia accounted for the additional 1.1 to 2.3 wt% above the theoretical hydrogen capacity of 8.2 wt%. Not only did Spex milling increase the ammonia release temperature but it also reduced the amount of ammonia released, further indicating the importance of particle size on desorption kinetics.

2.1.3. Isothermal Dehydrogenation/Hydrogenation Cycling of Unmodified System

The effect of synthesis methods on the rates of isothermal dehydrogenation and rehydrogenation of unmodified 1:1 $LiNH_2$:MgH_2 were investigated. The following cycling processes were used: dehydrogenation at 200 °C for 6 h into 1 bar of H_2 back pressure, and rehydrogenation under 100 bar of H_2 at 180 °C for 6 h. After observing the significant formation of Mg_3N_2 from dehydrogenation at 260 °C [30], the temperature was reduced to 200 °C to prevent ammonia loss. Previous investigations have shown that decreasing the temperature for hydrogenation/dehydrogenation effectively restrains the particle sizes of the samples, enhancing kinetics during cycling [29]. The isothermal hydrogen discharge data for both the Fritsch and Spex milled samples after the first and fourth discharge cycles are given in Figure 5. In order to study the rates of charge and discharge, the overall rate of grams of hydrogen per second discharged and charged was calculated during the first 30 min of the cycle.

Figure 5. Hydrogen desorption curves at standard desorption conditions during first and fourth isothermal discharge cycles of the unmodified material.
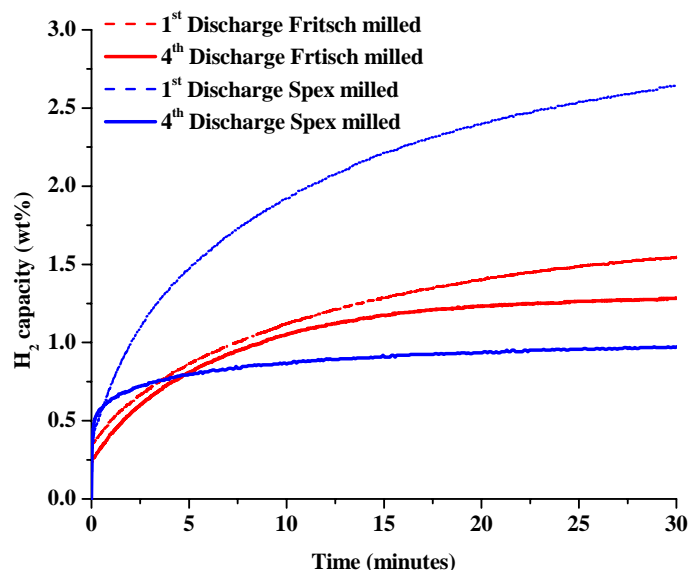
This produced the initial rate in [gH$_2$/s]/kg$_{material}$. This rate was then converted to bed discharge/charge rate using the estimated bed size, in kg, to determine the average absorption hydrogen capacity after 4 cycles. The 2010 DOE technical targets for onboard hydrogen storage for 5 kg of usable hydrogen are 3 gH$_2$/s for desorption and 20 gH$_2$/s for absorption [36]. These average rates are given as a function of cycle in Figure 6. The Spex milled sample initially showed significantly faster dehydrogenation rates than the Fritsch milled sample over 2 isothermal cycles at 200 °C. After the second cycle, the samples showed similar discharge kinetics at values significantly less than the technical target. The possible kinetic barriers to dehydrogenation are discussed below.

Figure 6. Overall bed discharge (**A**) and recharge (**B**) rate in gH$_2$/s for Spex (red) and Fritsch (blue) milled samples.
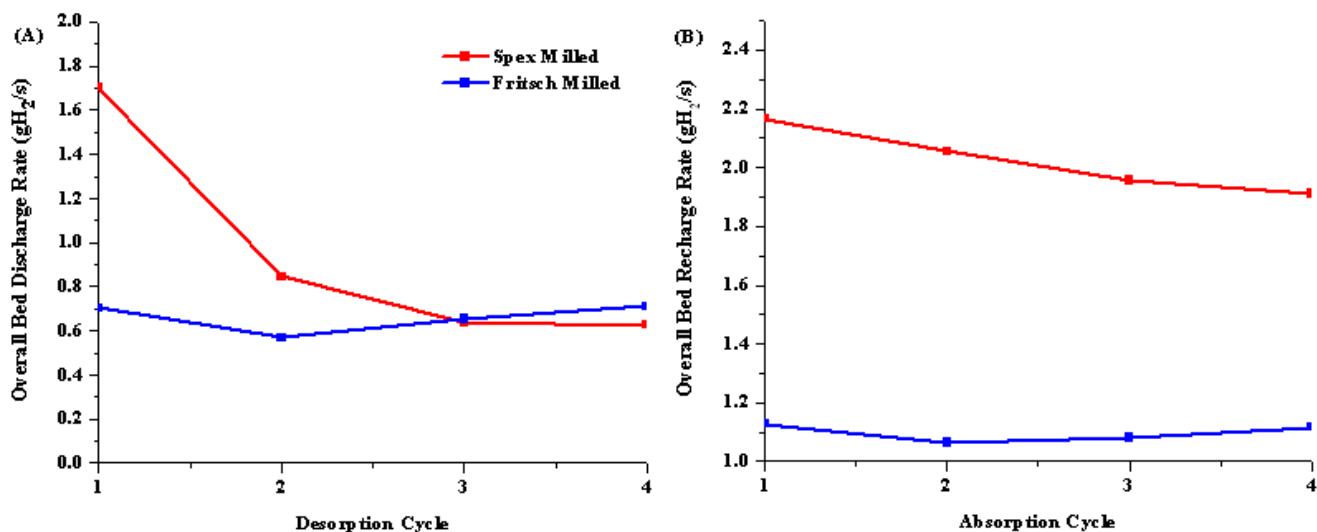
During rehydrogenation, the Spex milled sample was able to maintain a faster recharging rate than the Fritsch milled sample. Between dehydrogenation and rehydrogenation cycles, the sample was

cooled from 200 °C to 180 °C for 20 min while under active vacuum to fully dehydrogenate the sample. Spex milling initially improved the desorption rate close to the DOE technical target but was unable to improve the absorption rate past a tenth of the target.

The average absorption capacity for both materials was 4.4 wt%, which is half of the theoretical hydrogen capacity, indicating that partial dehydrogenation occurred at 200 °C. This correlates well with the TGA and hydrogen emission data seen during the initial decomposition for both samples, which showed one to two hydrogen releases prior to 300 °C and significant hydrogen release past 300 °C.

Both samples exhibited the same reduction in dehydrogenation capacity seen in our previous work [30]. This reduced capacity was attributed the reduction in diffusion kinetics for the transition metal halide modified mixtures to the formation of lithium salts, irreversible Mg_3N_2 formation, the loss of essential ammonia and the agglomeration of particles during the high temperature dehydrogenation [30]. However, in this experiment, the reduction kinetics can be attributed to the favorable reaction between LiH and N to form Li_2NH [37], essentially hindering the formation of necessary intermediate steps. A thermodynamic study is in progress to determine the changes in reaction enthalpy due to isothermal cycling.

2.1.4. Phase Identification

In order to identify the phases existing during the cycling process, an XRD analysis was performed after heating to 200 °C under pressure during the initial dehydrogenation cycle and after the fourth rehydrogenation cycle at 180 °C. The XRD pattern after heating shows that $LiNH_2$ had begun to decompose owing to the reduction of $LiNH_2$ peaks and formation of LiH peaks. There was no indication of MgH_2 decomposition, as illustrated in Figure 7.

Figure 7. XRD pattern of starting material after heating to 200 °C under 100 bar of pressure prior to dehydrogenation cycle.
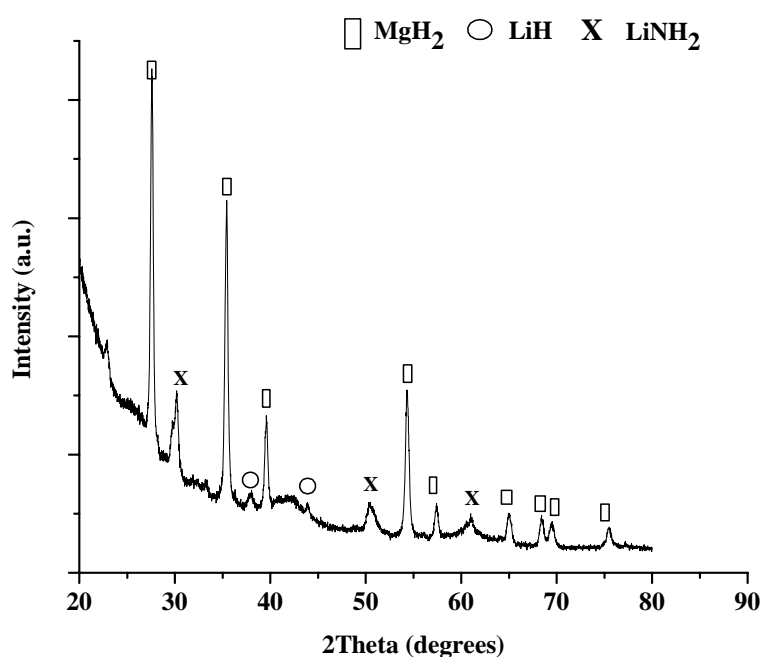
The XRD pattern, seen in Figure 8, of the cycled material shows that LiH and MgH_2 were the predominate products accompanied by Mg_3N_2 formation. The presence of Mg_3N_2 could indicate incomplete rehydrogenation under 100 bar at 180 °C. A future pressure dependence study will be conducted to confirm the sensitivity of the end products to cycling conditions.

Figure 8. XRD pattern of Spex (bottom) and Fritsch (top) milled 1:1 $LiNH_2$:MgH_2 after the 4th hydrogenation.
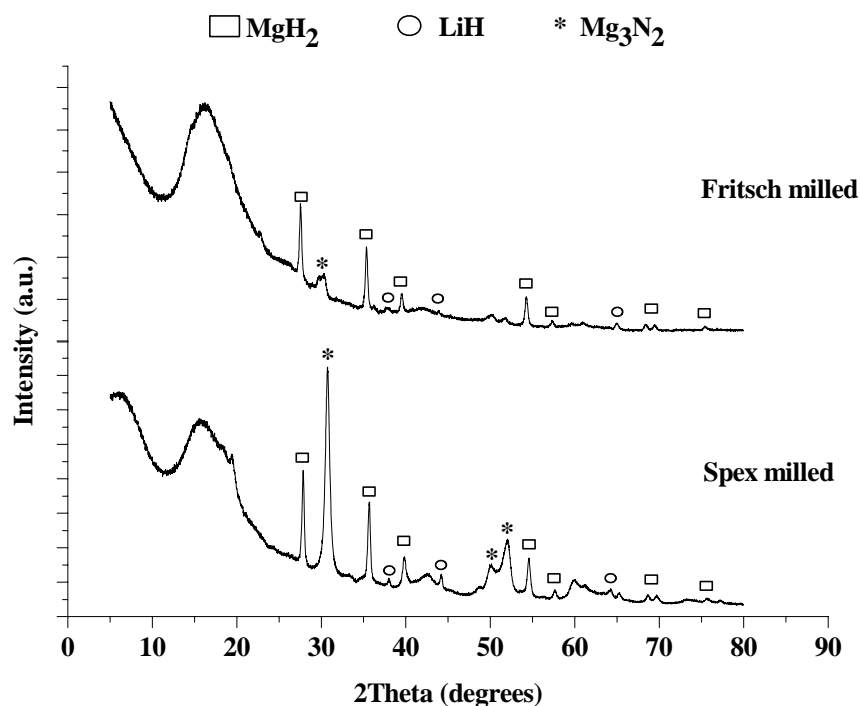
An increase in MgH_2 particle size after cycling was observed and calculated for each sample, as reported in Table 1. The particle size increased 20 nm due to cycling, indicating that particles agglomerated, potentially reducing the overall surface area and subsequently the kinetics of the system.

Table 1. Average particle size of MgH_2 before and after cycling.

Milling Conditions	Average MgH₂ Particle Size before Cycling (nm)	Average MgH₂ Particle Size after Cycling (nm)
Spex	23.6	43.5
Fritsch	35.3	49.8

$Mg(NH_2)_2$, another anticipated product of the reversible sorption reactions, is not identified possibly due to it being in an amorphous state. In the N–H stretching region of Raman spectroscopy, bands at 3273 cm^{-1} and 3326 cm^{-1} were observed, which are consistent with the formation of $Mg(NH_2)_2$ as seen in our previous publication [30].

2.2. Modified 1:1 LiNH₂:MgH₂ Systems

2.2.1. Characterization of As-Milled Modified Material

The XRD spectra of the as-milled Fe_2O_3 and V_2O_5, modified samples are given in Figure 9. It was concluded that oxide decomposition during milling did occur owing to the presence of MgO peaks. Using the Gibbs free energy of reactions between MgH_2 and V_2O_5 and Fe_2O_3, the reduction of the oxides by MgH_2 is predicted to be:

$$MgH_2 + Fe_2O_3 \rightarrow 2FeO + MgO + H_2 \qquad \Delta G = -279.6 \text{ kJ} @ 273 \text{ K} \tag{15}$$

$$3MgH_2 + V_2O_5 \rightarrow 2VO + 3MgO + 3H_2 \qquad \Delta G = -974.6 \text{ kJ} @ 273 \text{ K} \tag{16}$$

Therefore, both V_2O_5 and Fe_2O_3 can be reduced by MgH_2 possibly impacting the overall hydrogen capacity and kinetics of the modified systems. Thermodynamic data for the interaction between $LiNH_2$ and the oxides is not available at this time.

Figure 9. XRD patterns for the as-milled 1:1 $LiNH_2$:MgH_2 mixtures with 1.5 mol% V_2O_5 (bottom) or Fe_2O_3 modified materials.
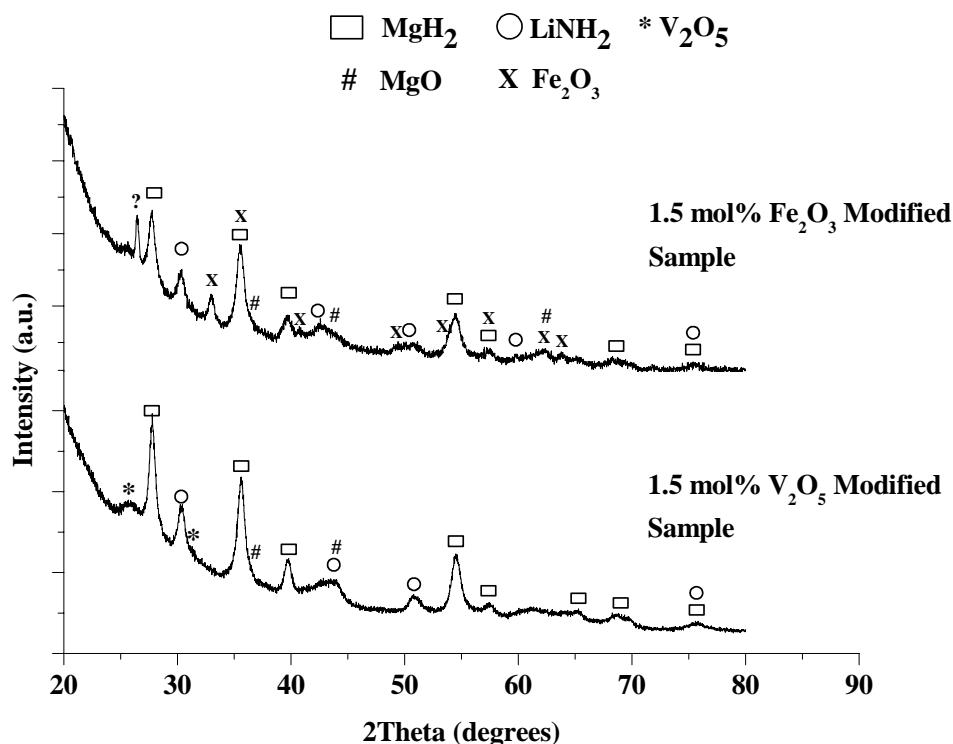
2.2.2. Decomposition Behavior of As-Milled Modified Material

Similar to the unmodified composition, two desorption reactions were also observed during the decomposition of the V_2O_5 and Fe_2O_3 modified 1:1 $LiNH_2$:MgH_2 mixtures. The temperature at which these reactions occurred and the amount of released hydrogen and ammonia for each reaction were dependent on modification composition. Figure 10 shows desorption TGA results ramping from RT to 400 °C under vacuum at 5 °C/min. With the addition of oxide modifier, the theoretical hydrogen capacity drops from 8.14 wt% to 7.45 wt% and 7.36 wt% for Fe_2O_3 and V_2O_5 modified sample, respectively.

Figure 10. TGA curves for unmodified (black), 1.5 mol% Fe_2O_3 (red) and V_2O_5 (blue) Spex milled 1:1 $LiNH_2$:MgH_2 mixture at 5 °C/min from 30 °C to 400 °C. The initial increase in weight observed during the start of the heating process is attributed to the expansion of the argon carrier gas.
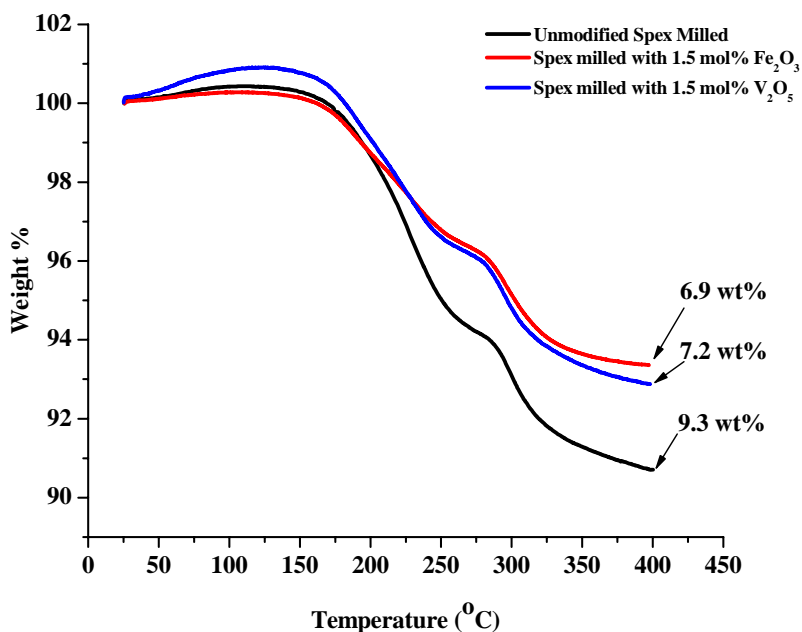
The weight loss of the Fe_2O_3 modified sample was 6.9 wt% and 7.2 wt% for the V_2O_5 modified sample, which are both close to their respective theoretical capacities, indicating that the dehydrogenation process was complete without significant NH_3 release. The difference from theoretical weight capacity is attributed to the possible reduction of the oxides by MgH_2, potentially releasing hydrogen during the milling process.

From the RGA data for these materials, the initial desorption resulted in two definable hydrogen release events and one ammonia release event. These are summarized in Table 2 with the first and second hydrogen release peaks designated H^1 and H^2. The two releases can be attributed to the interaction of the two decomposition reactions identified by Akbarzadeh *et al.* [4]. The addition of both Fe_2O_3 and V_2O_5 did effectively reduce the temperature of the two hydrogen release by 15 to 20 °C indicating its improvement on the desorption kinetics of the mixture. From literature, the observed improvement in kinetics is attributed to oxides of metals with multiple valence states, which promote the electronic exchange reactions with hydrogen molecules, accelerating the gas-solid reactions [38]. Typically the transition metal oxide modifier with more valance states proves to be more effective at impacting the sorption kinetics [39].

Table 2. Summary of TGA/RGA decomposition data of the as-milled samples without and with modifiers.

Compositional Modification	Theoretical H_2 Weight %	Total Weight % Released	H^1	H^2	Peak Ammonia Release Temperature
No Modification	8.2	9.3	240	345	285 °C
1.5 mol% Fe_2O_3	7.45	6.9	225	330	270 °C
1.5 mol% V_2O_5	7.36	7.2	220	325	270 °C

Figure 11. RGA curves for (**A**) hydrogen and (**B**) ammonia for as-milled unmodified (black), Fe$_2$O$_3$ (red) and V$_2$O$_5$ (blue) modified materials.
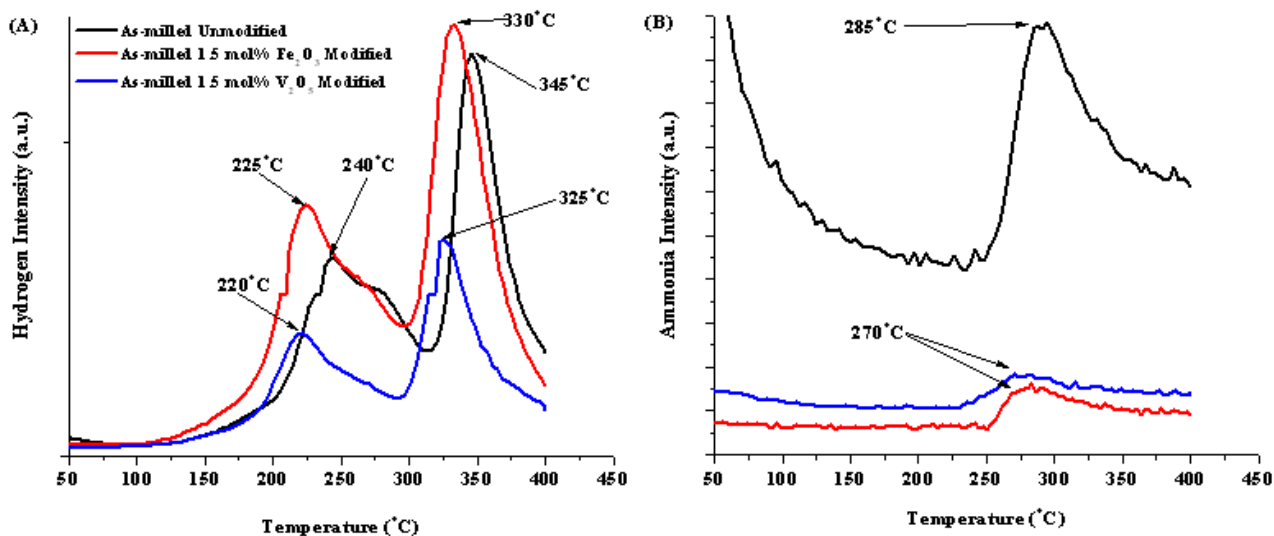
Compositional additions also greatly affected ammonia release. As seen in Table 2 and Figure 11B, both modifiers were effective at reducing the quantity of ammonia release during decomposition compared to the unmodified sample; however, the peak ammonia temperature was lowered by 15 °C. The mechanism behind this is not understood at this time.

2.2.3. Isothermal Hydrogenation/Dehydrogenation of Modified 1:1 LiNH$_2$:MgH$_2$ System

The impact of the transition metal oxide additions on the average bed discharge/recharging rates of isothermal dehydrogenation and rehydrogenation of 1:1 LiNH$_2$:MgH$_2$ were investigated under similar conditions to those listed in the previous section. From Figure 12A, the rate of discharge was not dependent on composition as seen by the similar continuous decrease in rate over four cycles for both the oxide modified and unmodified samples.

Figure 12. Bed discharge rate for unmodified (black), Fe$_2$O$_3$ (red) and V$_2$O$_5$ (blue) modified samples. The material was discharged under standard conditions.
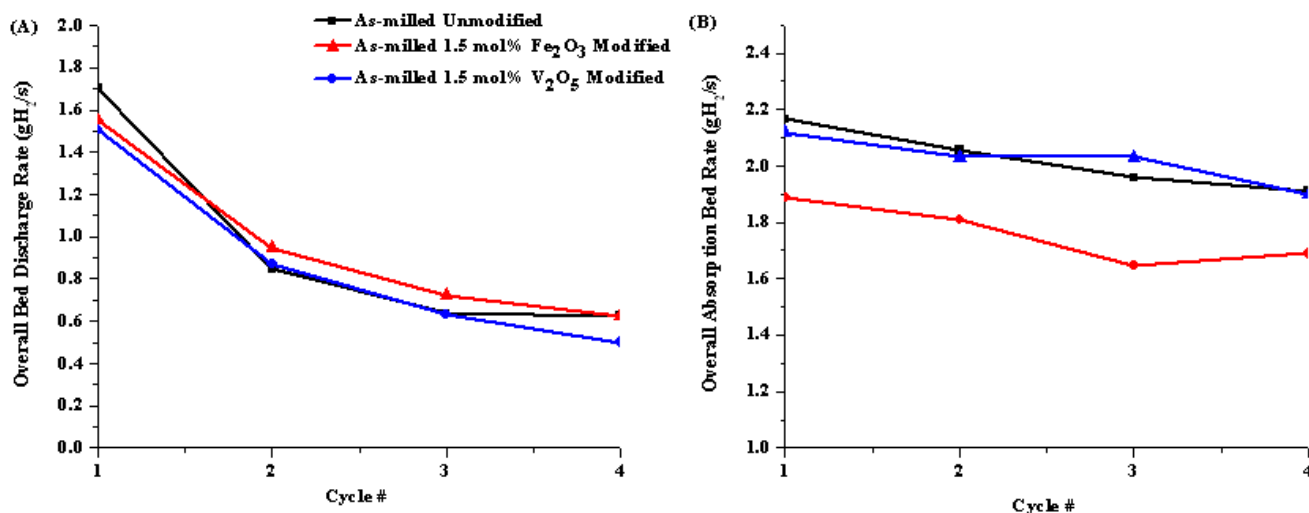
After the second isothermal dehydrogenation cycle, The Fe_2O_3 modified material showed slightly faster discharge kinetics than the unmodified and V_2O_5 modified samples. These are similar to literature results of discharging MgH_2 with different oxide catalysts at 300 °C into vacuum [38]. The reduction in discharge kinetics over four cycles can potentially be attributed to the exposure to high temperatures which leads to significant coarsening of the microstructure resulting in a slow-down of kinetics [40]. The authors went on to show that oxides have a larger impact on desorption of MgH_2 that absorption; therefore, the desorption cycle is more sensitive to catalyst deterioration [40]. Klassan *et al.* discussed that transition metal oxides showed more improvement on sorption kinetics than their pure metal counterparts [38], indicating that once the oxides are reduced during cycling, they lose their effectiveness [39].

2.2.4. Phase Identification after Cycling

Figure 13 gives the results of the XRD analyses performed after the fourth rehydrogenation cycle at 180 °C. The XRD spectra show that LiH, Mg_3N_2 and MgH_2 were the predominant products. Oxide deterioration was observed with the formation of MgO, VO and FeO peaks, confirmation of the thermodynamic analysis. However, similar to the unmodified samples, $Mg(NH_2)_2$ peaks were not identified due possibly to it being in an amorphous state.

Figure 13. XRD pattern of unmodified (bottom), V_2O_5 (middle) and Fe_2O_3 (top) modified 1:1 $LiNH_2$:MgH_2 after the 4th rehydrogenation cycle.
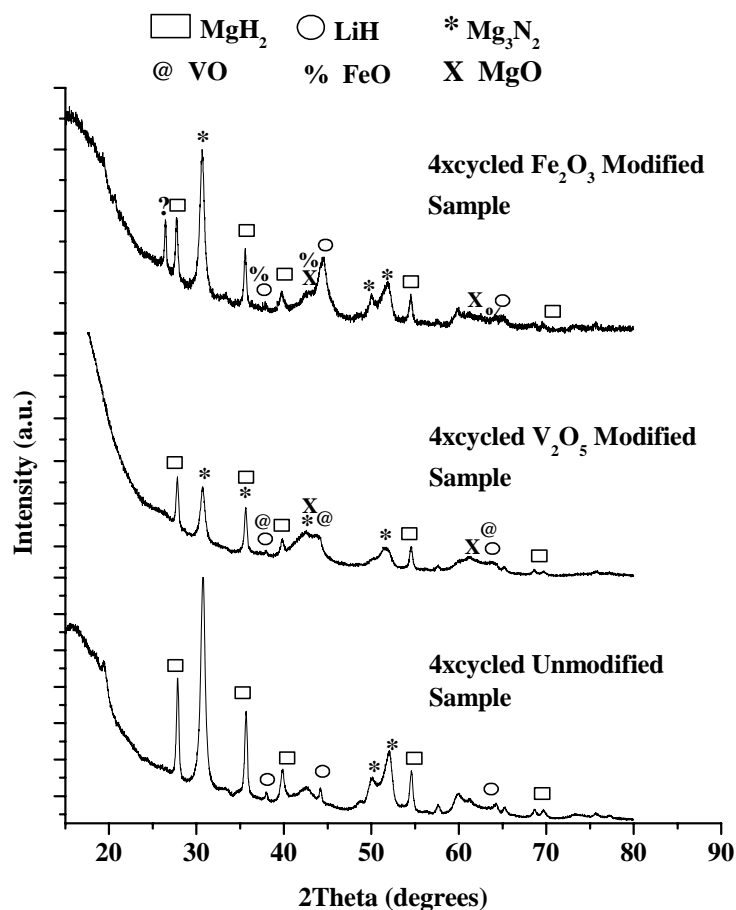
3. Experimental Section

The starting materials, lithium amide ($LiNH_2$, 95%, Aldrich), magnesium hydride (MgH_2, >97%, Gelest Inc.), vanadium oxide (V_2O_5, >99%, Aldrich) and iron oxide (Fe_2O_3, >99%, Aldrich) were purchased and used without alteration. Samples were prepared using a Fritch planetary or Spex milling technique. Three grams of 1:1 $LiNH_2$:MgH_2 without modifiers were loaded into the Fritsch milling jars while in the argon glove box. A 30:1 ball to sample weight ratio for the Fritsch mill and a 10:1 ratio for Spex milling were maintained. The Fritsch milled powders were milled for 2 h with 30 min cycles at 500 rpm while the Spex mill was also milled for 2 h in 30 min cycles.

Powder X-ray Diffraction (XRD) patterns of the as-milled, dehydrogenated and rehydrogenated materials were collected on a Rigaku Dmax/2100 (Cu K_α radiation). The samples were mounted on a glass slide and covered with Kapton® film while under argon. The XRD patterns were recorded from 2θ spanning 5 to 80° with a scanning rate of 0.02°/min.

Effluent gas composition was monitored as a function of temperature and time using a thermogravimetric analyzer (TGA) coupled with a residual gas analyzer (RGA). The TGA was located inside an argon glove box to prevent the samples from oxidizing. Five gram samples were loaded into a stainless steel microbalance pan and heated from 30 °C to 400 °C with a heating rate of 5 °C/min under a constant flow of argon gas. The effluent gases from the TGA were constantly monitored for H_2 (mass 2), NH_3 (mass 16 and 17), H_2O (mass 18) and O_2 (mass 32) gases using a Hiden Analytical residual gas analyzer (RGA).

Hydrogen desorption and absorption kinetics measurements were carried out using a Sievert's apparatus (PCTPro-2000, Setaram). Approximate 0.5 g samples were loaded into a stainless steel reactor vial and sealed in a glovebox. Standard isothermal discharge procedure called for heating of the sample under 110 bar or greater, based on the estimated equilibrium pressure using the enthalpy determined by Alapati *et al.* [22] and the entropy listed for the 2:1 $LiNH_2$:MgH_2 mixture at 210 °C by Markmaitree et al [34], in order to prevent side reactions to occur while heating. During heating from RT to 200 °C, the change in pressure of the sample reactor was noted in order to account for prematurely discharged H_2. Once 200 °C was reached, the sample was discharged into the largest reservoir (1170 mL) with a backpressure of 1 bar. During subsequent recharging cycles, the sample was cooled from 200 °C to 180 °C for 20 min under active vacuum and then exposed to 100 bar of H_2 pressure. During the dehydrogenation and hydrogenation cycles, sample temperature and reservoir pressures were recorded.

4. Conclusions

In this paper, we have compared the effects of ball milling techniques and compositional modifications on the dehydrogenation/rehydrogenation rates, the temperature of initial hydrogen release and the amount of ammonia released from unmodified and modified 1:1 MgH_2 and $LiNH_2$. Spex milling the mixture resulted in reduced ammonia release and relatively faster sorption kinetics resulting from particle size reduction and increase in defect density. The addition of Fe_2O_3 and V_2O_5 modifiers significantly reduced the amount of ammonia emission during the initial decomposition. After four isothermal sorption cycles, the V_2O_5 modified mixture showed faster sorption kinetics than

the Fe_2O_3 mixture, indicating possible higher stability and promotion of hydrogen absorption through a higher defect density. Further studies are needed to fully understand the cycling pathways and the role the transition metal oxides had in sorption kinetics.

Acknowledgements

References

1. Pinkerton, F.E. Decomposition kinetics of lithium amide for hydrogen storage materials. *J. Alloys Compd.* **2005**, *400*, 76–82.
2. Matsumoto, M.; Haga, T.; Kawai, Y.; Kojima, Y. Hydrogen desorption reactions of Li–N–H hydrogen storage system: Estimation of activation free energy. *J. Alloys Compd.* **2007**, *439*, 358–362.
3. Chen, P.; Xiong, Z.; Luo, J.; Lin, J.; Tan, K.L. Interaction of hydrogen with metal nitrides and imides. *Nature* **2002**, *420*, 302–304.
4. Akbarzadeh, A.R.; Ozoliņš, V.; Wolverton, C. First-Principles Determination of Multicomponent Hydride Phase Diagrams: Application to the Li–Mg–N–H System. *Adv. Mater.* **2007**, *19*, 3233–3239.
5. Luo, W.; Sickafoose, S. Thermodynamic and structural characterization of the Mg–Li–N–H hydrogen storage system. *J. Alloys Compd.* **2006**, *407*, 274–281.
6. Araujo, C.M.; Scheicher, R.H.; Ahuja, R. Thermodynamic analysis of hydrogen sorption reactions in Li–Mg–N–H systems. *Appl. Phys. Lett.* **2008**, *92*, 021907–021903.
7. Luo, W. $LiNH_2$–MgH_2: A viable hydrogen storage system. *J. Alloys Compd.* **2004**, *381*, 284–287.
8. Leng, H.Y.; Ichikawa, T.; Hino, S.; Hanada, N.; Isobe, S.; Fujii, H. New Metal−N−H System Composed of $Mg(NH_2)_2$ and LiH for Hydrogen Storage. *J. Phys. Chem. B* **2004**, *108*, 8763–8765.
9. Luo, W.; Rönnebro, E. Towards a viable hydrogen storage system for transportation application. *J. Alloys Compd.* **2005**, *404–406*, 392–395.
10. Xiong, Z.; Wu, G.; Hu, J.; Chen, P. Ternary Imides for Hydrogen Storage. *Adv. Mater.* **2004**, *16*, 1522–1525.
11. Hu, J.; Fichtner, M. Formation and Stability of Ternary Imides in the Li–Mg–N–H Hydrogen Storage System. *Chem. Mater.* **2009**, *21*, 3485–3490.
12. Janot, R.; Eymery, J.-B.; Tarascon, J.-M. Investigation of the processes for reversible hydrogen storage in the Li–Mg–N–H system. *J. Power Sources* **2007**, *164*, 496–502.
13. Weidner, E.; Dolci, F.; Hu, J.; Lohstroh, W.; Hansen, T.; Bull, D.J.; Fichtner, M. Hydrogenation Reaction Pathway in $Li_2Mg(NH)_2$. *J. Phys. Chem. C* **2009**, *113*, 15772–15777.

14. Dolci, F.; Weidner, E.; Hoelzel, M.; Hansen, T.; Moretto, P.; Pistidda, C.; Brunelli, M.; Fichtner, M.; Lohstroh, W. *In-situ* neutron diffraction study of magnesium amide/lithium hydride stoichiometric mixtures with lithium hydride excess. *Int. J. Hydrog. Energy* **2010**, *35*, 5448–5453.

15. Yang, J.; Sudik, A.; Wolverton, C. Activation of hydrogen storage materials in the Li–Mg–N–H system: Effect on storage properties. *J. Alloys Compd.* **2007**, *430*, 334–338.

16. Chen, P.; Xiong, Z.; Yang, L.; Wu, G.; Luo, W. Mechanistic Investigations on the Heterogeneous Solid-State Reaction of Magnesium Amides and Lithium Hydrides. *J. Phys. Chem. B* **2006**, *110*, 14221–14225.

17. Leng, H.; Ichikawa, T.; Hino, S.; Nakagawa, T.; Fujii, H. Mechanism of Hydrogenation Reaction in the Li–Mg–N–H System. *J. Phys. Chem. B* **2005**, *109*, 10744–10748.

18. Aoki, M.; Noritake, T.; Nakamori, Y.; Towata, S.; Orimo, S. Dehydriding and rehydriding properties of $Mg(NH_2)_2$-LiH systems. *J. Alloys Compd.* **2007**, *446–447*, 328–331.

19. Aoki, M.; Noritake, T.; Kitahara, G.; Nakamori, Y.; Towata, S.; Orimo, S. Dehydriding reaction of $Mg(NH_2)_2$–LiH system under hydrogen pressure. *J. Alloys Compd.* **2007**, *428*, 307–311.

20. Chu, L.; Yongfeng, L.; Kun, L.; Bo, L.; Mingxia, G.; Hongge, P.; Qidong, W. Reaction Pathways Determined by Mechanical Milling Process for Dehydrogenation/Hydrogenation of the $LiNH_2$–MgH_2. *Chem. A Eur. J.* **2010**, *16*, 693–702.

21. Nakamori, Y.; Kitahara, G.; Miwa, K.; Ohba, N.; Noritake, T.; Towata, S.; Orimo, S. Hydrogen storage properties of Li–Mg–N–H systems. *J. Alloys Compd.* **2005**, *404–406*, 396–398.

22. Alapati, S.V.; Johnson, J.K.; Sholl, D.S. Identification of Destabilized Metal Hydrides for Hydrogen Storage Using First Principles Calculations. *J. Phys. Chem. B* **2006**, *110*, 8769–8776.

23. Lu, J.; Fang, Z.Z.; Choi, Y.J.; Sohn, H.Y. Potential of Binary Lithium Magnesium Nitride for Hydrogen Storage Applications. *J. Phys. Chem. C* **2007**, *111*, 12129–12134.

24. Lu, J.; Choi, Y.J.; Fang, Z.Z.; Sohn, H.Y. Effect of milling intensity on the formation of LiMgN from the dehydrogenation of $LiNH_2$-MgH_2 (1:1) mixture. *J. Power Sources* **2010**, *195*, 1992–1997.

25. Liu, Y.; Zhong, K.; Gao, M.; Wang, J.; Pan, H.; Wang, Q. Hydrogen Storage in a $LiNH_2$–MgH_2 (1:1) System. *Chem. Mater.* **2008**, *20*, 3521–3527.

26. Liang, C.; Liu, Y.; Luo, K.; Li, B.; Gao, M.; Pan, H.; Wang, Q. Reaction Pathways Determined by Mechanical Milling Process for Dehydrogenation/Hydrogenation of the $LiNH_2$/MgH_2 System. *Chem. A Eur. J.* **2010**, *16*, 693–702.

27. Osborn, W.; Markmaitree, T.; Shaw, L.L. Evaluation of the hydrogen storage behavior of a $LiNH_2$ + MgH_2 system with 1:1 ratio. *J. Power Sources* **2007**, *172*, 376–378.

28. Michel, K.J.; Akbarzadeh, A.R.; Ozolins, V. First-Principles Study of the Li–Mg–N–H System: Compound Structures and Hydrogen-Storage Properties. *J. Phys. Chem. C* **2009**, *113*, 14551–14558.

29. Liu, Y.; Zhong, K.; Luo, K.; Gao, M.; Pan, H.; Wang, Q. Size-Dependent Kinetic Enhancement in Hydrogen Absorption and Desorption of the Li–Mg–N–H System. *J. Am. Chem. Soc.* **2009**, *131*, 1862–1870.

30. Price, C.; Gray, J.; Lascola, R.; Anton, D. The Affects of Halide Modifiers on the Sorption Kinetics of 1:1 $LiNH_2$:MgH_2. *Int. J. Hydrog. Energy* **2010**, in press.

31. Bald, C.P.; Hereijgers, B.P.C.; Bitter, J.H.; de Jong, K.P. Sodium Alanate Nanoparticles-Linking Size to Hydrogen Storage Properties. *J. Am. Chem. Soc.* **2008**, *130*, 6761–6765.

32. Varin, R.A.; Jang, M.; Polanski, M. The effects of ball milling and molar ratio of LiH on the hydrogen storage properties of nanocrystalline lithium amide and lithium hydride (LiNH2 + LiH) system. *J. Alloys Compd.* **2010**, *491*, 658–667.

33. Markmaitree, T.; Osborn, W.; Shaw, L.L. Comparative studies of reaction rates of NH_3 with MgH_2 and LiH. *J. Power Sources* **2008**, *180*, 535–538.

34. Markmaitree, T.; Osborn, W.; Shaw, L.L. Comparisons between MgH_2- and LiH-containing systems for hydrogen storage applications. *Int. J. Hydrog. Energy* **2008**, *33*, 3915–3924.

35. Luo, W.; Stewart, K. Characterization of NH_3 formation in desorption of Li–Mg–N–H storage system. *J. Alloys Compd.* **2007**, *440*, 357–361.

36. DOE Targets for Onboard Hydrogen Storage Systems for Light-Duty Vehicles. Available online: http://www1.eere.energy.gov/hydrogenandfuelcells/storage/pdfs/targets_onboard_hydro_storage.pdf (accessed on 1 December 2010).

37. Hu, Y.H.; Ruckenstein, E. Ultrafast Reaction between LiH and NH_3 during H_2 Storage in Li_3N. *J. Phys. Chem. A* **2003**, *107*, 9737–9739.

38. Barkhordarian, G.; Klassen, T.; Bormann, R. Fast hydrogen sorption kinetics of nanocrystalline Mg using Nb_2O_5 as catalyst. *Scripta Mater.* **2003**, *49*, 213–217.

39. Huang, Z.G.; Guo, Z.P.; Calka, A.; Wexler, D.; Lukey, C.; Liu, H.K. Effects of iron oxide (Fe_2O_3, Fe_3O_4) on hydrogen storage properties of Mg-based composites. *J. Alloys Compd.* **2006**, *422*, 299–304.

40. Dehouche, Z.; Klassen, T.; Oelerich, W.; Goyette, J.; Bose, T.K.; Schulz, R. Cycling and thermal stability of nanostructured MgH_2–Cr_2O_3 composite for hydrogen storage. *J. Alloys Compd.* **2002**, *347*, 319–323.